

# High Accuracy Coronagraph Flight Model For WFIRST–CGI Raw Contrast Sensitivity Analysis

Hanying Zhou\*, John Krist, Eric Cady, Ilya Poberezhskiy  
Jet Propulsion Laboratory/California Institute of Technology,  
4800 Oak Grove Drive, Pasadena, CA 91109 USA

## ABSTRACT

A high-accuracy high-fidelity flight wavefront control (WFC) model is developed for detailed raw contrast sensitivity analysis of WFIRST-CGI. Built upon features of recently testbed validated model, it is further refined to combine a full Fresnel propagation diffraction model for high accuracy contrast truth evaluation, and an economical compact model for WFC purposes. Extensive individual raw contrast error sensitivities are evaluated systematically, both as known imperfections and as unknown calibration errors, for both spectroscopy mode and wide field-of-view mode with shaped pupil coronagraph. More than 90 distinct error items were identified, including system aberrations, optical misalignment, component manufacturing error, telescope interface related errors, etc. The result forms the basis for raw contrast error budget flow down to a sub-system level, where detailed specifications needed to aid in component design and manufacturing, mechanical alignment and instrument integration, and verification and validation operations. Evaluations are mostly automated, making it relatively easy for repeat runs of revised design or at new desired error quantity. Top error sensitivities and contrast floor contributors are discussed and several observations are noted.

**Key words:** Coronagraph, raw contrast sensitivity, error budget, wavefront sensing and control, coronagraph modeling, exoplanets, WFIRST, high contrast imaging

## 1. INTRODUCTION

NASA's planned Wide-Field Infrared Survey Telescope (WFIRST) mission is scheduled to transition from Phase A to Phase B, with CoronaGraph Instrument (CGI), one of the two instruments, being re-baselined as a technology demonstration recently. CGI operates in one of three modes: Hybrid Lyot Coronagraph (HLC) imaging with narrow field-of-view (FoV), Shaped Pupil Coronagraph (SPC) integral field spectroscopy (IFS), and SPC imaging with wide FoV. Various performance requirements have been under development and underwent review recently [1-4]. The current CGI performance budget, done for each mode, consists loosely of five categories such as static contrast, contrast stability, throughput, measurement noise, and telescope interface [1]. Raw contrast, along with contrast stability, is the next most important performance metric after throughput for current CGI design [5]. Raw contrast affects contrast stability as well through the cross-term with dynamic stability [6]. Unlike stability error budget, which has been a frequent subject and primary focus for various coronagraph designs and architectures [4-7], raw contrast sensitivity (and its error budget) has not been systematically studied with a model based analysis. This is partially because contrast stability is often what drives the engineering requirements *if* assuming a very high raw contrast to start with. The fact that getting sensitivity matrix of raw contrast is much more computationally demanding (as it requires WFC iterations for accurate assessment) does not help either. On top of these, it also had been difficult to accurately predict a real system's raw contrast performance until very recently.

During the past years, significant effort and progress have been made in advancing the model fidelity for an as-built coronagraph system's raw contrast and contrast sensitivities predictions [8-11]. For example, good agreements (within 35%) have been demonstrated for SPC between testbed results and model predictions in three main aspects of contrast performance metrics: raw contrast floor, contrast convergence rate, and contrast sensitivities to low order Zernike wavefront error (WFE) among others [9]. The key to the improved model fidelity comes from two aspects: 1) better / more thorough knowledge of actual system (in this case it was chromatic system aberrations rather than simple achromatic ones), and 2) incorporation of WFC features as in use, such as electric field sensing through pair-wise probing, deformable mirror

(DM) voltage constraints and actuator neighbor-rules as enforced on testbed to prevent potential mirror damage from large strokes on adjacent actuators, regular update of control matrix and active regularization strategy, etc.

The purpose of this work is to provide a comprehensive model based raw contrast sensitivity analysis in support of CGI error budgeting (raw contrast is one major supporting lower-level error budget during recent CGI system requirement review). In the following we describe our high accuracy shaped pupil coronagraph flight model and sensitivity analysis tool developed. We begin with general description of our model configuration and setting, evaluation method and error terms, and some implementation details. This is followed by the highlights from evaluation results, and a brief discussion on how permissible amounts of various errors are allocated at subsystems and components level (Levels 5 & 6). Details on high level CGI performance error budget development can be found elsewhere [1-3], while a related end-to-end CGI modeling to validate these performance budgets is in [12].

## 2. SPC FLIGHT WFC MODEL CONFIGURATION

### 2.1 Flight optical layout and SPC coronagraph masks

The current Phase A flight CGI optics design is similar to the one used on JPL’s High Contrast Imaging Testbeds (HCIT) where most of our model validation work data came from. The main difference is the actual front end telescope optics replaces the OTA (optical telescope assembly) simulator used on HCIT. Figure 1 shows the schematic of the WFIRST telescope and CGI optics for two SPC modes that are the subjects of this work. From telescope’s primary and secondary mirrors (PM, SM or T1, T2 in the figure), to fast steering mirror (FSM) where CGI optics begins, to imager plane, total of more than 30 optical elements are involved in current optics layout (excluding LOWFS and IFS arm optics). More detailed description of flight telescope and CGI optics can be found in [13].

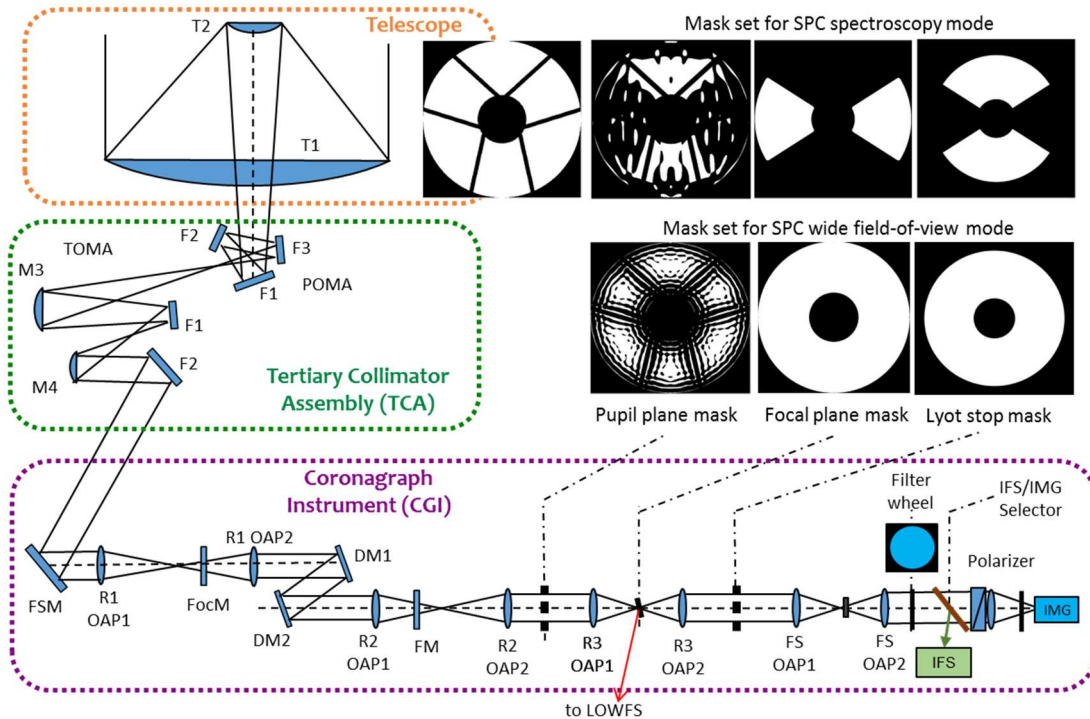


Figure 1. Schematic of WFIRST-CGI optics layout as used in Phase A flight model. All lenses except the IFS/IMG selector are mirrors, unfolded for display purposes. FSM: fast steering mirror; FocM: focus correction mirror; FM: fold mirror; OAP: off-axis parabola; DM: deformable mirror; LOWFS: low order wavefront sensing; IFS: integral field spectroscopy; IMG: imager plane; TOMA: tertiary optical mirror assembly; POMA: pickoff optical mirror assembly.

Also shown in Figure 1 (upper right portion) are telescope pupil and the SPC flight mask sets used in this work: the spectroscopy mode (20170714, top right row) and wide FoV mode (20170130, top right second row) [14]. Note that the WFIRST telescope pupil has since changed and will require a new round of mask design which will occur in Phase B. The shaped pupil coronagraph uses a binary pupil mask, together with a focal plane mask and Lyot stop, to alter the star's diffraction pattern and achieve a desired dark hole at image plane. Its simple design renders it relatively insensitive to jitter and chromaticity, among others. Unlike in previous generation, the Lyot stop in current design for spectroscopy mode is no longer of annular shape but of 90° rotated bowtie-like shape. This improves throughput. The current design also has extra padding for strut width in an attempt to reduce pupil/beam shear sensitivity found in past, and it explicitly optimizes tip/tilt sensitivity and a few others during the design process as well. Additionally, current designs take consideration of existing PM's aberration rolloff at edge.

## 2.2 SPC Flight WFC Model Setup

The core flight optical system model has been detailed elsewhere [12]. We highlight a few main features here along with some adjustments made (to tailor for sensitivity analysis).

Prior to current work, a preliminary detailed raw contrast error budget flow-down analysis was performed [3] which used a similar SPC spectroscopy mask design (20170501), HCIT's testbed-like system aberrations, and our lab validated model where a compact model was used for both contrast truth evaluation and control matrix (aka Jacobian) calculation (we will label this version as "HCIT flight"). For current Phase A flight model, we aim to further improve our model to be realistic in representation of flight system's aberrations and constraints, accurate in error sensitivity assessment (e.g. of many mask-related error items), and capable of individual error item evaluation as desired.

To achieve this we combined a full model and a compact model for our flight model. Specifically, we used a full Fresnel propagation diffraction model and full mask design size (1000 pixels) and large (4×) zero padding for FFT for contrast truth evaluation (*Full PROPER contrast model*). In this full model beam propagates from surface to surface according to the layout's physical distances, picking up aberration at each surface along the way. MFT (Matrix Fourier Transform, [15]) was used in place of FFT to magnify field to highly sampled focal plane. For WFC Jacobian calculation (*EFC control model*), we used an economical compact model, with reduced mask size (500 pixels) and less zero padding (2×) for FFT. The compact model starts from DM1 (a pupil plane), Fresnel propagates from DM1 to DM2 (and back to DM1), and after multiplying with the shaped pupil mask it uses MFT to both focal mask plane and Lyot stop plane. A final sampling of 0.2 is used for spectroscopy mode while a 2× coarser one was used for wide FoV imaging mode. These steps were intended to reduce the computational burden, reflecting the computing resource constraint of the future flight system. (CGI baselines onboard computation for the future flight WFC control software, in which Jacobian calculation is a significant bottleneck due to limited flight processors).

Since the flight telescope and CGI is yet to be built, aberrations used in the full model for contrast consist of mostly synthetic ones. Care is taken that they match manufacturer's specs where possible except for existing primary and secondary mirrors where measured ones used. Additional low-order aberration is added at FSM to account for the front end telescope optics alignment error, bringing overall WFE to that of expected observatory level performance. Besides these, we also include polarization-induced chromatic aberrations (due to polarization coupled with coating and angle dependent Fresnel reflection), which was found to be critical in past modeling [9, 12]. Polarization coefficients for representative wavelengths are precalculated using Code V ray-tracing result of current WFIRST-CGI optics and coating properties. They are then interpolated as needed in the model. Note that in order to fully utilize the limited throughput but excellent achromaticity nature of SPC, current CGI baselines no polarizer in both of its two SPC modes. To simulate this, four polarized in/out pairs of light channels are propagated individually in the full model: +45° incident polarization in, 0° and 90° out, and -45° in, 0° and 90° out (i.e., each of the two orthogonal polarizations is coupled into the polarization orthogonal to the input one). Contrast is then calculated as the average of all four channels (the E field can be obtained simply by using the mean of the four polarization aberration maps without separate propagations). More details on how those aberration maps are generated can be found in [12].

Besides optics figure imperfections, we also included testbed like alignment imperfection, particularly the DM registration, in both full diffraction model and compact control model. Other system constraints include DM maximum voltage and neighbor rule constraints (e.g., less than 30V difference for any neighboring pair of actuators) [9].

For the compact control model, the individual surface aberrations are compressed into a single entrance pupil aberration and estimated from the full model up to shaped pupil plane (the downstream optics are ignored as they have little effect on contrast). Note that, for Jacobian calculation, only field knowledge is needed but not contrast. Therefore no individual polarization channel propagation is needed. The compact control model uses estimated chromatic WFE from the full model for each wavelength, as if measured by a phase retrieval method in a real system.

The WFC method used is the standard image-plane based electric field conjugation (EFC) algorithm [16, 17]. In this method, the control matrix is a collection of linear approximation of (model based) image plane electric field response to each (pupil plane) actuator's unit-strength poke. At each iteration, the system's actual E field is obtained through a pair-wise DM probing procedure. We note however due to time constraint, this probing is not routinely used as a tradeoff from the need of full size full Fresnel propagation and polarization effect, both of which increase the computation time substantially. As a result, the E field is now assumed to be perfectly sensed/estimated during EFC; the imperfect sensing is then evaluated as a separated error item. Also while many new WFC strategies are being investigated and tested out, such as extra tip tilt control, Kalman filtering, Jacobian compensation, refined regularization strategy, etc., none is baselined yet for flight SPC, and therefore are not used in current flight model.

As in the past, our flight WFC model was developed with the PROPER diffraction modelling tool [18 -20] for the optical system evaluation and MATLAB in general for WFC and others. The error items and their quantities are organized with an Excel spreadsheet, with types of error -- known error ("alignment error"), unknown error ("knowledge error"), or open loop -- and levels of error (0.5deg, 0.1% or 1um, 1nm, etc.) specified, as illustrated in Table 1 below.

Category	Type	Name	Short name	size	units
Telescope pupil	Alignment	Strut width change	strut width	0.1	% of tel D
Polarization	Knowledge	rms delta Z4 from system polarization (+/- to ends of band)	chrn wfe Z4	1	nm
Telescope pupil	Knowledge	Strut width change	strut width	0.1	% of tel D
Polarization	Open-loop	rms delta Z2 from system polarization (+/- to ends of band)	chrn wfe Z2	1	nm
Polarization	Open-loop	rms delta Z3 from system polarization (+/- to ends of band)	chrn wfe Z3	1	nm
Polarization	Open-loop	rms delta Z4 from system polarization (+/- to ends of band)	chrn wfe Z4	1	nm
Polarization	Open-loop	rms delta Z5 from system polarization (+/- to ends of band)	chrn wfe Z5	1	nm
Polarization	Open-loop	rms delta Z6 from system polarization (+/- to ends of band)	chrn wfe Z6	1	nm
Starting system wavefront	Open-loop	rms Z2 at FSM	pup wfe Z2	1	nm
Starting system wavefront	Open-loop	rms Z3 at FSM	pup wfe Z3	1	nm
Starting system wavefront	Open-loop	rms Z4 at FSM	pup wfe Z4	1	nm
Starting system wavefront	Open-loop	rms Z5 at FSM	pup wfe Z5	1	nm
Telescope pupil	Open-loop	Pupil clocking (edge only, no WF)	pup clocking	0.1	deg
Telescope pupil	Open-loop	Pupil shear X (edge only, no WF)	pup xshear	0.1	% of tel D
Telescope pupil	Open-loop	Pupil shear y (edge only, no WF)	pup yshear	0.1	% of tel D
Telescope pupil	Open-loop	WF clock	beam clocking	0.01	deg
Telescope pupil	Open-loop	WF shear X	beam xshear	0.1	% of tel D
Telescope pupil	Open-loop	WF shear Y	beam yshear	0.1	% of tel D
Mask alignment relative to nominal	Alignment	shaped pupil mask X	sp xshift	10	um
Mask alignment relative to nominal	Alignment	shaped pupil mask Y	sp yshift	10	um
Algorithm calibration	Knowledge	Plate scale	plate scale	0.05	L/D
DM actuator calibration	Knowledge	DM gain calibration uncertainty	dm dgain	5	%

Table 1. Example of error items organized in spreadsheet.

The analysis routine is automated as illustrated in Figure 2. First a reference dark hole speckle field is obtained through EFC iterations beforehand with all system's baseline aberrations, misalignment, and constraints in place as described above. The sensitivity analysis then runs in an automated looped fashion. The software script reads in one error item at a time from spreadsheet, converts it into a quantity with an appropriate unit and decides if to run a full EFC course, and if to include error knowledge in Jacobian calculation or other appropriate places, or if to use the post EFC dark hole DM solution associated with the reference dark hole field and check the effect of perturbation (open loop). Error is applied to the system on top of its baseline conditions, and the perturbed field is obtained in one of the three options. It then compares the result field to the reference field from pre-saved reference file for field sensitivity squared,  $|E|^2$ , and output contrast sensitivity result to a pre-specified output spreadsheet file. The sensitivities are calculated per subband wavelength (five for spectroscopy, and three for wide FoV imaging), per sub radial dark hole region (generally three). All EFC courses are

run for fixed 100 iterations (roughly the current typical testbed EFC iterations) with fixed regularization for fair and accurate comparison. Upon finishing the evaluation of the current error item, it moves on to the next one on the spreadsheet list automatically.

Throughout the paper, we use “contrast” in its loose definition, which is actually “normalized intensity” (i.e., the speckle intensity normalized by the PSF peak at origin without including coronagraphic focal-plane mask throughput). Contrast is generally worse than normalized intensity near the inner working angle by this definition, but sensitivity is not much different.

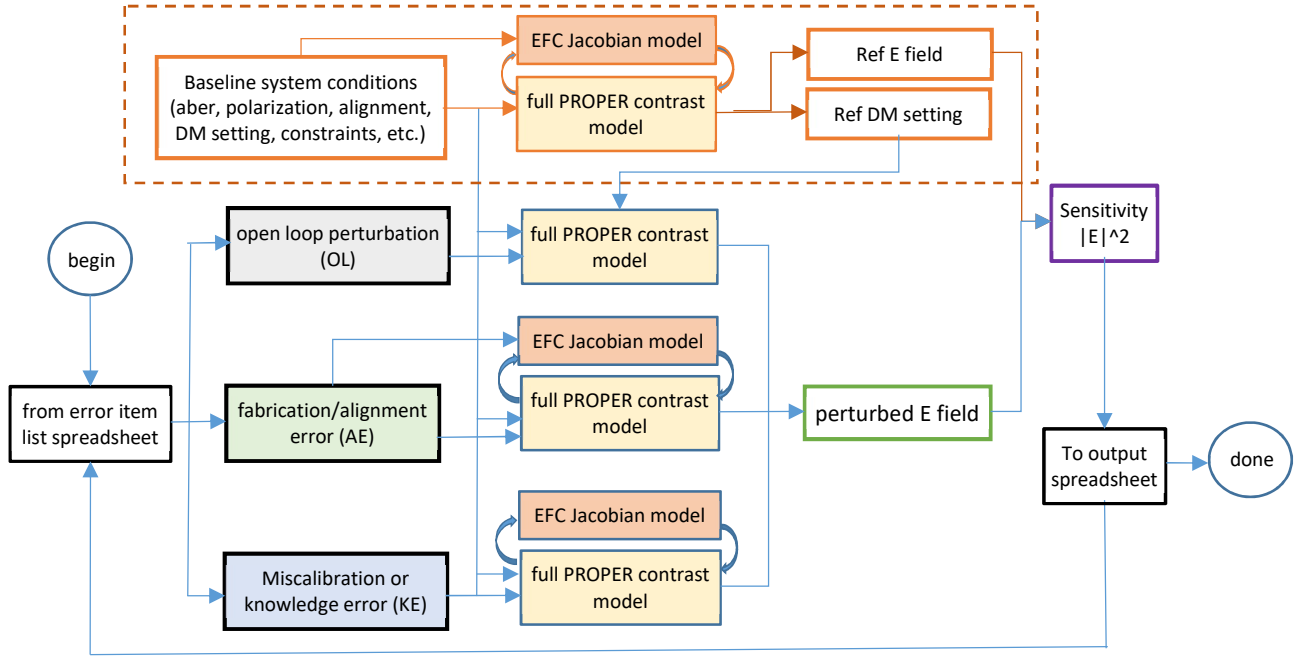


Figure 2. Automated analysis routine. The dashed part is precalculated, the rest is a looped execution. The *full PROPER contrast model* is used for high accuracy contrast evaluation, while *EFC Jacobian model* for economical Jacobian calculation

### 3. ERRORS TERMS AND IMPLEMENTATION NOTES

The focus of this paper is on the raw contrast (closed-loop, CL) sensitivities, though open loop (OL) sensitivities were also performed along the way; the former determines the modulated part of raw contrast while some latter terms determines the unmodulated part of raw contrast. Since CGI employs an iterative WFC scheme, it can help overcome many imperfections in system (to a degree) if they are known and if iterations go on long enough. It may be less capable of doing so if it is an unknown imperfection (knowledge error). We thus distinguish errors into three different types based on whether or how an error is applied with or without WFC process: as **known** error that is incorporated into both the fast control model and the high-fidelity system representation, as **unknown** error which is included in the high-fidelity representation but not the control model, and as **open loop perturbation** to a post EFC dark hole (that is, it does not subject to further EFC iteration). A more practical reason for this distinction is that the error budget derived is intended to go to different engineering teams and/or stages of the flight CGI lifetime: specifications for teams who designs, manufactures, and integrates components into an instrument (“misalignment and fabrication”, or **alignment error** for known errors); and specifications for teams who conduct the verification & validation test or dark hole (DH) digging operations post CGI integration (“miscalibration”, or **knowledge error** for unknown errors). In the following, we mostly use the latter designations (and their abbreviations) of error types (**O** or **OL** for open loop, **A** or **AE** for alignment error, and **K** or **KE** for knowledge error).

More than 90 distinct individual error terms were identified by system engineers and evaluated here for both spectroscopy and wide FoV modes, covering most major components/elements of the instrument. They can be loosely grouped in four

categories as listed in Table.2: 1) optical alignment error; 2) component fabrication errors; 3) system aberrations; and 4) front end telescope interface related error. Note that, in both modes, our flight model stops at the imaging-camera plane and our sensitivity analysis captures error items up to imaging-camera only. IFS part optics error sensitivities are not included in this work but captured in a separate performance assessment and error budget [21].

Category	Error Names	Typical Qty	Numbers & Types of eval
Telescope Interface	Pupil (edge) clocking	0.1 deg	3; OAK
	Pupil (edge) lateral shear	0.1%D	6; OAK in x and y
	Beam (wavefront ) clocking	0.1%D	3; OAK
	Beam (wavefront) shear	0.1deg	2; O, in x and y
	Strut width	0.1%D	3, OAK
	Pupil magnification	1%D	3; OAK
	Secondary mirror diam	1%D	3; OAK
	Pointing / source lateral offset	0.1 $\lambda$ /D	6; OAK; in x and y
Optical Misalignment or Mismatch	Deformable mirror tip/tilt/clocking	[0.5 0.5 0.1] deg	18; OAK; DM1, DM2
	Deformable mirror lateral and axial offset	[10 10 1000] um	14; OAK; DM1, DM2
	Shaped pupil mask tip/tilt/clocking	[0.5 0.5 0.1] deg	9; OAK;
	Shaped pupil mask lateral and axial offset	[10 10 10] um	9; OAK; in x,y, and z
	Focal-plane mask tip/tilt/clocking	[0.5 0.5 0.1] deg	9; OAK;
	Focal-plane mask lateral and axial offset	[10 10 10] um	9; OAK; in x,y, and z
	Lyot tip/tilt/clocking	[0.5 0.5 0.1] deg	9; OAK;
	Lyot lateral and axial offset	[10 10 10] um	9; OAK; in x,y, and z
	Beam magnification at focal-plane mask	1%	3; OAK
	Beam magnification at shaped pupil	1%	3; OAK
	Beam magnification at Lyot stop	1%	3; OAK
Component Fabrication or Usage	Shaped pupil mask undercut	1%	1; K
	Focal-plane mask inner, outer radius	1um	2; K;
	Focal-plane mask angle extend & offset	[0.5 0.5]deg	2; A;
	Lyot stop inner, outer radius	1um	2; K;
	Shaped pupil mask magnification	1%	1; A
	Shaped pupil mask surface WFE	1nm	1; A
	Deformable mirror actuator gain	5%	1;K
	Deformable mirror quantization	16 bit DAC	1; K
	Deformable mirror thermal offset	10 mk	1; OK
System Aberrations	Achromatic wavefront error Z2~Z4, at fast-steering mirror	1nm	3; O
	Chromatic wavefront error Z2~Z6, at fast-steering mirror	+/- 1nm	15; OAK
	Achromatic amplitude error Z2~Z6+, at DM1	1%	18; OAK
	Chromatic amplitude error Z2~Z6+, at DM1	+/-1%	18; OAK
	wavefront error at DM1, Z4~Z8+	1nm	18; OAK
	wavefront error at shaped pupil, Z4~Z8+	1nm	18; OAK
	wavefront error at Lyot stop, Z4~Z8+	1nm	6; O
Algorithm	Plate scale	0.05 $\lambda$ /D	1; K
			Total: ~ 233

Table 2. Error items evaluated for SPC spectroscopy modes.  
*O* as open loop error; *A* as alignment error; and *K* as knowledge error

The following are some of implementation notes.

- **Mask lateral shift:** This includes shaped pupil, focal-plane, and Lyot stop masks. To provide accurate subpixel shift, we generally apply equivalent tilt in FT domain, multiply the mask, FFT back, then remove the tilt out (applying a negative tilt).
- **Shaped pupil mask clocking and magnification:** The shaped pupil mask has many delicate edges. To alleviate potential digital implementation error for clocking and magnification, we FFT a  $4\times$  zero-padded mask, rotate or magnify it in the Fourier domain where a more smooth rotation / magnification is possible than in the mask spatial domain directly, and then FFT back.
- **Shaped pupil undercut:** For each non-interior pixel, we assign a reflection magnitude drop (relative to 1) based on how much area it loses for a specified amount of undercut from an overetch during black-silicon processing [22]. The loss in area depends on how many open neighbors it has and the locations of the undercut sides.
- **Beam magnification and mask magnification (mismatch):** These are two different types of beam size and mask size mismatch: the former refers to the incorrect beam size than expected (e.g., from misaligned optics) but mask is correctly manufactured; the latter refers to correct beam size but incorrectly manufactured mask. In implementation, the former essentially resizes wavefront size, while the latter resizes a mask in Fourier domain (see above).
- **Telescope pupil/beam lateral shear:** We evaluated pupil lateral shear in two slightly different concepts: as pupil (mask edge) shift, and as beam shear with wavefront loaded. The former is shifted upfront in model at the telescope entrance pupil by using a pupil drawing tool to give precise shift (reflecting mostly the effect of portion of telescope element, e.g., secondary mirror strut position alignment). For the beam shear, we shift wavefront loaded beam laterally at the FSM plane, simulating a possible beam walk due to telescope pointing or telescope - CGI interface breakup where telescope itself is treated as a rigid body.
- **DM registration, gain, and voltage constraints:** When there is knowledge error (i.e., “unknown”) in calibration of DM registration, gain, or just apply the voltage constraints, care must be taken in model that these errors become “known” even if the errors are labeled as knowledge error. This is because one typically starts with DM “flattening” before EFC. The “flattening” itself is an iterative process with help of phase retrieval measurement. DM registration error or gain error or voltage constraints are implicitly “worked out” for this flatten part DM. The unknown error should only be applied to the subsequent EFC portion of DM.
- **Aberrations for compact control model:** Here we assume the flight system aberrations for compact control model are obtained through PR measurement post DM flattening. In this scenario, both known and unknown aberration errors become effectively “known” through the flattening process and are then fed to compact control model through estimation procedure.

Total over ~230 individual error evaluations performed for spectroscopy mode, with each individual error item in one or all three types of errors (KE, AE, OL). For wide FoV mode, we evaluated most KE and OL cases but skipped AE cases, with total ~100 error evaluations.

#### 4. PERFORMANCES AND DISCUSSIONS

Before we go into details on sensitivities results, some quick comments on our compact control model. For all the evaluations in this work we used an “economical” compact model for Jacobian to make sure the results obtained are more or less realistically achievable under limited computing resource anticipated for the on-board flight software. As a result the control Jacobian is less than perfect (compared to full mask sized compact model). In fact the relative error (in magnitude) between the Jacobian with the economical model and that of a full sized compact model is about 7% on average

for DM1, and 15% for DM2, skewed by a few extreme large errors from edge actuators of weak Jacobian magnitudes ( DM2 is less impactful than DM1 due to much small stroke magnitude involved). To see if there is significant loss by using such an economical model, we compared the baseline EFC contrast by the control model we currently use and that of a full size compact model. The difference is minor: 1.25e-9 vs 1.21e-9 mean contrast, economical vs full size control models. No extensive comparison on sensitivity was done but it is expected to be even smaller difference due to differential nature. This indicates our economical compact model for Jacobian purpose for the two SPC modes is reasonably adequate. Although Jacobian can be efficiently improved if one uses larger mask and FFT padding sizes for edge actuators only, we opt not to do this for this study. We want to stress that this is by no means an optimal setting for future flight Jacobian which will require an extensive modeling and testing on its own.

Table 3 lists some baseline raw contrast performances (mean, coherent) for both spectroscopy mode and wide FoV imaging mode. These include ideal design contrast without any aberrations, aberrated (with current best estimate) contrast before low-order static correction (DM flattening), post low-order correction contrast, and post high-order EFC correction contrast. In both modes, the post EFC contrasts (the last columns in Table 3) with a model uncertainty factor (MUF) of 2 will be taken as “design contrast” in error budget breakdown tree (see in Sect.4.5).

Tables 4 & 5 summarize the most sensitive (relative to some common error quantities) error terms for each mode as simulated. Allocations are chosen appropriately so the error budget closes in the presence of these tall tentpoles.

mode	band & bandwidth	DH region	ideal design	aberrated	post flatten	post EFC
spectroscopy	band 3 (760nm), 18%	2.5 ~9λ/D	2.06E-09	4.4E-04	2.3E-06	1.3E-09
wide FoV imaging	band 4 (825nm), 10%	6.5 ~20λ/D	8.00E-10	4.3E-05	1.7E-06	6.3E-10

Table 3. Baseline raw modulated contrast for spectroscopy mode and for wide FoV imaging mode

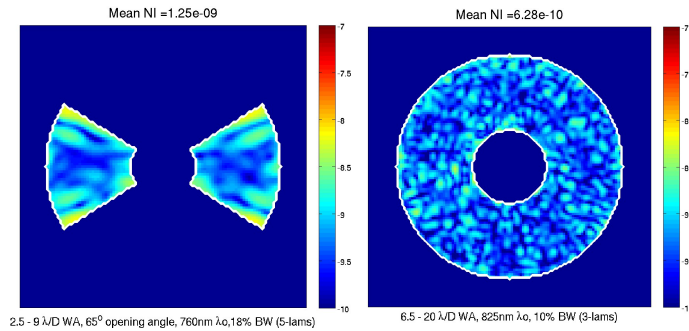


Figure 3 Baseline post EFC raw modulated contrast for spectroscopy mode (left) and for wide FoV mode (right)

Error Names	Qty	3-4 λ/D	4-5 λ/D	5-8 λ/D	avg
chromatic WFE Z4	+/-1nm	3.9E-10	1.2E-10	1.9E-10	2.3E-10
chromatic WFE Z5	+/-1nm	7.3E-11	3.3E-11	6.0E-11	5.5E-11
chromatic WFE Z6	+/-1nm	2.9E-11	1.1E-11	2.5E-11	2.2E-11
chromatic amp Z4	+/-1%	2.9E-10	9.5E-11	1.4E-10	1.8E-10
chromatic amp Z5	+/-1%	7.9E-11	3.1E-11	7.9E-11	6.3E-11
chromatic amp Z6	+/-1%	9.1E-11	5.1E-11	7.8E-11	7.4E-11
chromatic amp> Z6	+/-1%	4.3E-09	1.1E-09	1.9E-09	2.4E-09
shaped pupil mask clocking	0.5deg	1.6E-10	1.6E-10	5.1E-10	2.8E-10
shaped pupil mask xtilt	0.5deg	4.9E-11	4.0E-11	9.0E-11	6.0E-11
shaped pupil mask mag	0.5%	1.1E-11	1.6E-11	2.2E-11	1.6E-11
focal-plane mask clocking	0.5deg	1.1E-11	1.1E-11	5.2E-11	2.5E-11
beam mag at shaped pupil	0.5%	1.5E-11	1.5E-11	1.9E-11	1.6E-11

DM quantization                      16 bitDAC      1.1E-11      9.9E-12      1.7E-11      1.3E-11

Table 4. Spectroscopy mode raw contrast sensitivity tall tentpole

Error Names	Qty	6.5-7.5 $\lambda/D$	7.5-19 $\lambda/D$	19-20 $\lambda/D$	avg
chromatic amp dm1 > Z6	+/-1%	3.9E-10	1.4E-11	1.3E-11	1.4E-10
shaped pupil mask clocking	0.5deg	1.3E-09	7.1E-10	9.6E-10	1.0E-09
shaped pupil undercut	5%	7.5E-11	1.8E-11	2.7E-11	4.0E-11
beam mag at shaped pupil	0.50%	7.2E-11	3.4E-11	6.0E-11	5.5E-11
beam mag at shaped pupil	-0.50%	1.4E-09	2.0E-10	4.9E-10	7.0E-10
shaped pupil mask mag	0.50%	1.2E-10	3.6E-11	8.3E-11	8.0E-11
shaped pupil mask mag	-0.50%	2.7E-10	5.1E-11	9.1E-11	1.4E-10
pupil mag	1% ofD	1.7E-11	1.6E-11	1.5E-11	1.6E-11

Table 5. Wide FoV mode raw contrast sensitivity tall tentpole

Several observations can be made from the comprehensive error evaluations.

#### 4.1 Phase A Flight vs “HCIT Flight”

Compared to our earlier sensitivity matrix and error budget derived from it [3] where a similar SPC spectroscopy mask design but HCIT-like system aberration was used (“HCIT Flight”), we saw majority (of the ~75 items evaluated both times) of error sensitivities are similar or improved. In fact, slightly more than half error items has 2× or better sensitivities, and just a short of third have similar sensitivities to its predecessor. These improvements likely come from a combination of factors, like a smaller overall system aberrations (see Figure 4), a longer wavelength used (which further renders most errors relatively moderate), and a generally-more-accurate contrast model this time. Only less than one fifth are more sensitive. Among this last group, one is chromatic WFE and amplitude; the other is pupil and SP clocking.

The relatively poorer (3~5×) chromatic WFE and amplitude sensitivities (than in earlier analysis [3]) is because we are now dealing with a little bit more challenging polarization situation: earlier analysis did not have a polarization model *per se* (though it did include chromatic WFE). Now not only a longer wavelength is used and so a bit higher polarization level exists, but more importantly since no polarizer is used, there is incoherent mixing of four polarizing light channels for dark hole contrast.

As for the slightly poorer pupil and shaped pupil mask clocking, a possible reason is that the current flight aberration has a relatively larger WFE near the edge at pupil (see Figure 4) due to large optics used (PM and SM). Previous HCIT-like aberration used much smaller optics for the OTA simulator. The large edge WFE requires large DM stroke at edge, in turn making it slightly more sensitive to clocking-type error.

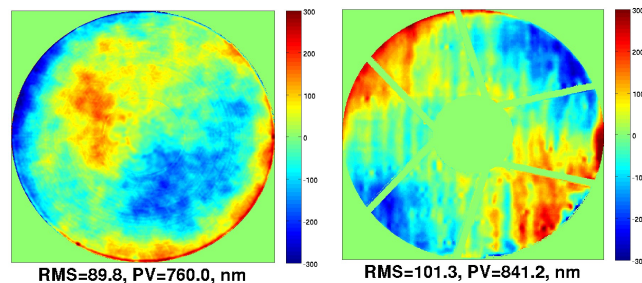


Figure 4. Left: Phase A flight system pupil WFE (compressed up to shaped pupil plane); Right: measured HCIT testbed measured WFE used in previous analysis

#### 4.2 Spectroscopy mode vs wide FoV mode

For spectroscopy mode, some of the biggest contrast-floor contributors come from chromatic WFE and amplitude (due to polarization coupled with Fresnel reflection). This is consistent with what we discovered previously during testbed WFC model validation efforts [9]. Some shaped-pupil-mask related errors, particularly clocking, are next major contrast-floor contributors; so are bowtie mask clocking and DM quantization.

Wide FoV mode, however, is notably more susceptible to shaped-pupil-mask related error items than its spectroscopy counterpart. For example, shaped-pupil-mask clocking at  $0.5^\circ$  is  $\sim 3\times$  more sensitive, beam and shaped-pupil-mask size mismatch at 0.5% is  $\sim 5\times$  more sensitive, and shaped pupil undercut at 1um is  $\sim 7\times$  worse than their counterparts of spectroscopy mode. This is because shaped pupil mask for wide FoV has much more edge perimeter than the spectroscopy mode design. For the same error quantity like  $0.5^\circ$  clocking, the affected area is larger than in spectroscopy case (see Figure 5 below), hence more contrast degradation. As to chromatic WFE due to polarization, although it has big impact on spectroscopy, the effects are mostly of low order, and therefore has less impact for wide FoV mode whose dark hole region is in more a mid-frequency range. Chromatic amplitude, although among most sensitive, is expected to be of much smaller magnitude in practice than  $\pm 1\%$  standard quantity evaluated here, and therefore not of particular practical concern.

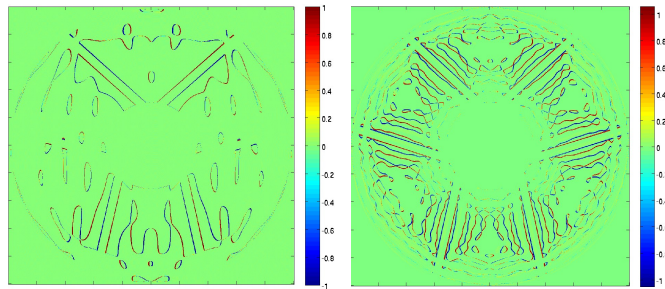


Figure 5. For a given error quantity ( $0.5^\circ$  clocking here), shaped pupil mask for spectroscopy mode (left) has less edge length, and hence less error area than that for the wide FoV mode (right)

#### 4.3 Known Error vs Unknown Errors

Surprisingly, sensitivities of these two types of error differ very little under current conditions. The majority of error items have negligible difference between the two; only a few items have noticeable difference (i.e., Lyot stop), but even in these cases the absolute sensitivity level is low and so not critical. (As a result, we skipped Alignment Error evaluation for wide FoV mode, using Knowledge Error sensitivities as conservative surrogates). We suspect a possible reason for the lack of difference is that due to iterative nature, the EFC process compensates the deficit in knowledge at the small error level we evaluated. If the unknown is large, whether as a single factor (e.g., the missed chromatic WFE information in the testbed modeling work, [9]) or as a cumulative effect (most real system), it may change this similarity. Currently the individual error is added on top of a perfectly known model of baseline conditions. On testbeds and in future flight condition, many unknowns coexist. The behavior may change if the accumulated error is large, and evaluating this is the work of future modeling.

#### 4.4 Full contrast model vs compact contrast model

Obviously the full model (for contrast evaluation) has the ability to evaluate error items that a compact model is incapable of or difficult to perform, such as optical axial position accuracy for DMs, shaped pupil mask, occulter mask, and Lyot Stop mask. Besides these, the full model also serves as a way to cross check accuracies of various compact models or even analytic estimation of sensitivities. It is expected that the full model provides better accuracy than compact model for certain error items that may have location dependency to some degree.

To illustrate this we constructed a compact model for contrast evaluation purpose (which is separate from the compact model used for Jacobian calculation). We used the same mask size and FFT padding size as in the full contrast model. The system aberrations are estimated from the full model up to shaped pupil plane. Using the same Jacobian calculated with economical compact model, the baseline raw contrast for spectroscopy mode is  $\sim 2.04e-9$  for perfect design

(unaberrated and no EFC), almost the same as in full model. It degrades to about  $4.57e-4$  for the aberrated system, and improves back to about  $\sim 1.31e-9$  with EFC. In other words, the baseline aberrated post EFC contrasts are considered close enough. However, we saw significant difference on two open loop sensitivities we tested: the compact model overestimate the beam (wavefront) shear sensitivity by a factor of  $4\times$ , but underestimate the pupil (edge) shear by a factor of  $\sim 5\times$ . We believe the reason for the former is that in full model the WFE is distributed among optics and therefore could be less severe up to FSM plane (since it have not accumulated all the optics after it up to shaped pupil plane). In the compact model, system aberration input is a compressed one from full model that is placed right at DM1 plane. Similarly, the reason for pupil (edge) shear is that the diffraction (at telescope strut) at the front location of telescope has a cascading effect in the full model while in compact model it does not engender more propagation.

These results have implications for future V&V tests, as this example shows one needs to make clear what (a pupil mask, or a wavefront loaded beam) and where (at the fast steering mirror or other positions) is being rotated.

As a side note, while the post EFC contrasts are of similar level from their respective evaluations, the final dark hole DM solution from the full contrast model based EFC course and that from the compact contrast model differ slightly (see Figure 6). For a high contrast coronagraph however, this small DM difference is enough to have a huge consequence. In fact if one interchanges the dark hole DM solution between the two contrast models, the contrast drops from  $1.3e-9$  to  $9.3e-7$  or from  $1.25e-9$  to  $1e-6$ . This could explain a testbed phenomenon that the measured raw contrast at the end of EFC tends to be very different from (typically a few orders of magnitude better than) its control model would predict. Note that the testbed EFC process can be viewed more as an approximation of a full contrast model + an economical EFC model, than an approximation of a single or two compact models (for contrast evaluation and EFC process respectively). If one uses DM solution achieved on testbed (the true contrast, as represented by the full contrast model here) into its control model (similar to the compact contrast model), it is not self consistent and so results in poor contrast. Much effort has been poured into the Jacobian (control matrix) mismatch issue and its improvement on testbed. This study shows that the mismatch in the electric field representation may also have a role in testbed EFC process and deserve further investigations.

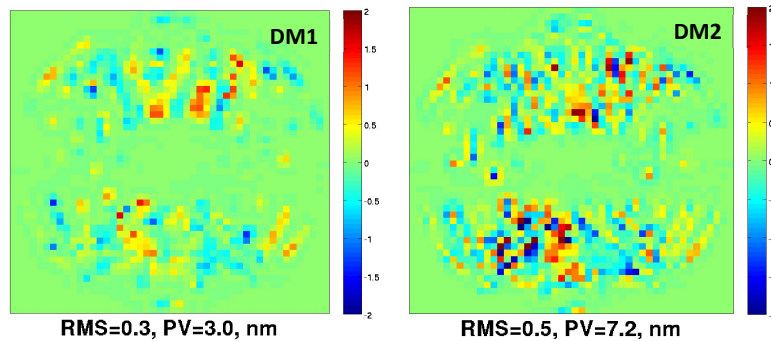


Figure 6. Difference between final dark hole DM solutions of full contrast model and of compact contrast model (both use the same economical EFC control model); The full DM strokes range  $\sim 230\text{nm}$  PV for DM1,  $\sim 30\text{nm}$  PV for DM2

#### 4.5 Raw Contrast Error Budget Flowdown

Here we briefly summarize the initial raw contrast error budget flowdown to the engineering parameters at subsystem level. Discussions on higher level performance budget can be found [1-3].

The raw contrast requirement is consisted of two main parts: coherent and incoherent contrast contributions. The coherent part starts from the design contrast with baseline system conditions, and includes contrast contributions from two types of errors: misalignment / fabrication errors and miscalibration errors, whose detailed lists are summarized in Table 2 and are the main subject of this work. Their results are used straightforwardly in the error budget flowdown process. As illustrated in Figure 7, for each error item, a permissible allocation is assigned based on its calculated sensitivity and engineering feasibility or constraints. A contrast is then scaled for the allocated amount of error with a Model Uncertainty Factor (MUF). Typically MUF of 2 is applied for most of these sensitivity terms per project policy. Finally contrast is summed up linearly [6] for all the adjusted contrasts to meet (iteratively) the raw contrast of the top level performance.

The incoherent part of contrast includes both static and dynamic contributions that cannot be discerned through slow DM modulation for wavefront sensing, such as telescope jitter, finite source size, polarization, stray light and background light, estimation error, etc.; many of them can be evaluated based on OL sensitivity results with little extra calculation. For example, jitter and stellar size related sensitivities are aggregated sensitivities from time or spatially (incoherent) average of many tip/tilted intensities. Both are found to be proportional to the sum of half tip and tilt sensitivities, and are multiplied by the magnitude of jitter squared, or the effective stellar size squared. A few terms are not yet modeled and are represented by contrast allocations to that error source. The most impactful sub-item among them is the high order jitter.

An example of the rolled up error budget tree for wide FoV mode is shown in Figure 8. Similar error budget tree for spectroscopy mode exists but not shown here. They are both parts of the supporting error budget during recent CGI system requirement review / system design review. A more detailed description of the CGI error budgeting, including raw contrast portion, can be found in [1].

Level C	Allocation	Sensitivity							Contrast		
		3-4 L/D	4-5 L/D	5-8 L/D	per	[unit]	MUF	estimated contribution per allocated	section contrast rollup		
Misalignment and fabrication									4.23E-09	1.83E-09	2.94E-09
<b>Mask alignment relative to nominal</b>		<b>ROLLUP</b>							<b>1.49E-10</b>	<b>1.33E-10</b>	<b>3.13E-10</b>
shaped pupil mask X	10 um	1	9.94E-13	1.03E-12	2.36E-12	10.00	um	2	1.99E-12	2.06E-12	4.71E-12
shaped pupil mask Y	10 um	1	9.18E-13	1.25E-12	2.43E-12	10.00	um	2	1.84E-12	2.50E-12	4.86E-12
shaped pupil mask Z	100 um	1	4.02E-15	4.01E-15	1.01E-14	10.00	um	2	8.04E-13	8.02E-13	2.03E-12
shaped pupil mask clocking	0.1 deg	1	1.15E-10	1.19E-10	3.67E-10	0.50	deg	2	9.23E-12	9.50E-12	2.93E-11
shaped pupil mask tip	0.5 deg	1	4.90E-11	4.00E-11	9.00E-11	0.50	deg	2	9.80E-11	8.00E-11	1.80E-10
shaped pupil mask tilt	0.5 deg	1	1.70E-14	2.21E-14	8.65E-14	0.50	deg	2	3.40E-14	4.42E-14	1.73E-13

Figure 7. Example of permissible error allocations and contrast contributions roll up (spectroscopy mode)

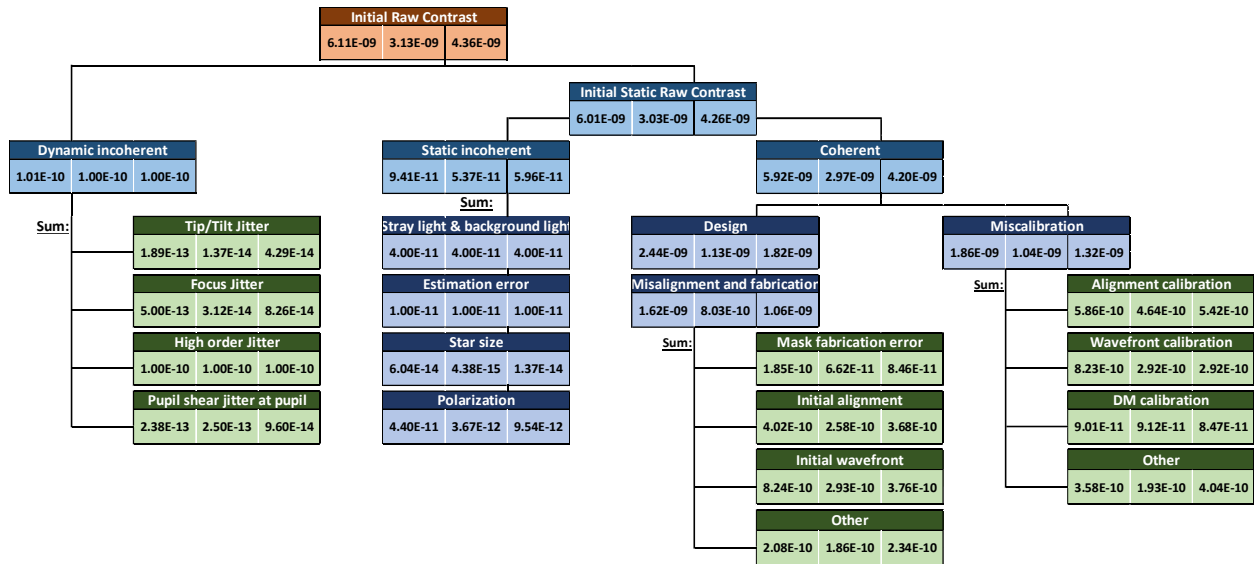


Figure 8. Example of raw contrast error budget tree, wide field-of-view imaging mode

## 5. SUMMARY AND FUTURE WORK

We have developed a high accuracy, high fidelity flight model and an automated analysis routine for shaped pupil coronagraph raw contrast sensitivity analysis in support of CGI error budget requirement development. A total of 90 error items identified and evaluated as either known error or unknown error or open loop perturbation, totaling 230+ evaluations

performed for spectroscopy mode and 100+ for wide FoV mode. The sensitivity analysis from this work forms the basis for CGI error budget flowdown to the subsystem level (Levels 5&6), such as mechanical, I&T, WFC, and component design and fabrication, etc.

Current results shows that for spectroscopy mode, chromatic WFE (due to polarization and Fresnel reflection) is among main raw contrast floor contributors followed by shaped pupil mask errors. For wide FoV mode, shaped pupil mask related errors are more prominent. A full contrast model is desirable for accurate prediction of sensitivity (as well as raw contrast itself) while an economical compact EFC model is adequate in achieving contrast. Different characteristics of system aberration may lead to some sensitivity change (e.g., clocking). Calibration errors have similar impact on contrast floor as known imperfections if they are small enough.

While extensive error items have been evaluated, the study is by no means complete. A few errors recently emerged as potentially critical have not been included in this analysis. Example includes DM influence function shape error.

As WFIRST-CGI enters Phase B, new mask design will be necessary for the updated telescope pupil. Flight conditions such as low flux, computation constraints, etc., may place more restrictions on how WFC will be carried out. Desires for a faster EFC (less iterations) or extra on and off axis tip tilt control for potential better open loop sensitivity will also affect WFC strategy. It likely will be necessary to re-evaluate raw contrast sensitivity with all these new realities and constraints and better WFC scheme to ensure any new tall tent poles are captured. The use of an automated error-budgeting routine will permit this to be done efficiently and repeatedly.

## ACKNOWLEDGMENTS

This work was performed at the Jet Propulsion Laboratory of the California Institute of Technology, under contract with the National Aeronautics and Space Administration. © 2018 California Institute of Technology. Government sponsorship acknowledged. The decision to implement the WFIRST mission will not be finalized until NASA's completion of the National Environmental Policy Act (NEPA) process. This document is being made available for information purposes only.

## REFERENCES

- [1] Poberezhshiy, I., et al., "WFIRST CGI: performance predictions for an active space coronagraph.", Proc. SPIE, 10698, 10698-244, this conference (2018)
- [2] Douglas, E. S., et al., "WFIRST: Update on the Coronagraph Science Requirements," AAS meeting 231, ID # 355.14 (2018)
- [3] Poberezhshiy, I., et al., "WFIRST: Coronagraph systems engineering and performance budgets.", AAS Meeting #231, ID# 361.13 (2018)
- [4] Noecker, M., et al., "WFIRST: managing telescope wavefront stability to meet coronagraph performance ," AAS meeting 231, ID # 246.35 (2018)
- [5] Nemati, B., et al., "HabEx telescope WFE stability specification derived from coronagraph starlight leakage," Proc. SPIE, 10698, 10698-119, this conference (2018)
- [6] Shaklan, S. B. et al., "The terrestrial planet finder coronagraph dynamics error budget," SPIE 5905, 59050D, 2005
- [7] Shaklan, S. B. et al., "Stability error budget for an aggressive coronagraph on a 3.8m telescope," SPIE, 8151, 815109, 2011
- [8] Zhou, H., et al., "Closing the Contrast Gap between Testbed and Model Prediction with WFIRST-CGI Shaped Pupil Coronagraph," Proc. SPIE. 9904, 9904-19,(2016)
- [9] Zhou, H., et al., "Wavefront control performance modeling with WFIRST shaped pupil coronagraph testbed", Proc. SPIE, 10400, 10400-5, (2017)
- [10] Marx, D., et al., "Electric field conjugation in the presence of model uncertainty," Proc. SPIE 10400, 10400-23, (2017).
- [11] Sidick, E., et al., "Sensitivity of WFIRST coronagraph broadband contrast performance to DM actuator errors," Proc. SPIE 10400, 10400-6 (2017).
- [12] Krist, J., "WFIRST coronagraph flight performance modeling", *Proc. SPIE*, 10698, 10698-90, this conference (2018).
- [13] Tang, H., et al., "The WFIRST coronagraph instrument optical design update," Proc. SPIE. 10400, 10400-2 (2017)

- [14] Riggs, A.J., et al., "Shaped pupil coronagraph design developments for the WFIRST coronagraph instrument," Proc. SPIE, 10400, 10400-73, (2017)
- [15] R. Soummer, L. Pueyo, A. Sivaramakrishnan, and R. J. Vanderbei, "Fast computation of Lyot-style coronagraph propagation," Opt. Express **15**, 15935-15951 (2007)
- [16] Give'on, A., et al., "Broadband wavefront correction algorithm for high-contrast imaging system," Proc. SPIE. 6691, 66910A (2007).
- [17] Give'on, A., et al., "Pair-wise, deformable mirror, image plane-based diversity electric field estimation for high contrast coronagraph," Proc. SPIE. 8151, 815110-2, (2011)
- [18] Krist, J., "PROPER: an optical modeling program for IDL," Proc. SPIE 6675, 66750P (2007).  
Also: <http://proper-library.sourceforge.net>
- [19] Krist, J., "End-to-end numerical modeling of AFTA coronagraphs", Proc. SPIE, 9143, 91430V (2014).
- [20] Krist, J., et al., "WFIRST coronagraph optical modeling," Proc. SPIE, 10400, 10400-4, (2017)
- [21] Groff, T., et al., "The IFS for WFIRST CGI: science requirements to design", AAS Meeting #231, ID# 355.47 (2018)
- [22] Balasubramanian, K., et al., "WFIRST-AFTA coronagraph shaped pupil masks: design, fabrication, and characterization," J. Astron. Telesc. Instrum. Syst. 2(1) 011005 (2015)